

Evaluation of GPS Indoor Positioning using Real Measurements and a One-Shot Software Receiver

Gustavo López-Risueño, Gonzalo Seco-Granados, Alberto García-Rodríguez
TTC and Navigation Section (TEC-ETT), Electrical Engineering Department
European Space Agency (ESTEC)
2201 AZ Noordwijk ZH, The Netherlands
Email: {gustavo.lopez.risueno,gonzalo.seco.granados,alberto.garcia}@esa.int

Abstract— In this paper, we evaluate the accuracy that GPS can provide indoors by processing live GPS L1 C/A signal recordings obtained in different indoor environments. A One-Shot software receiver is utilised to compute the fixes in an off-line mode. It has both coherent correlation and non-coherent integration for low-sensitivity purposes, interpolation for code delay estimation, a proper CN_0 estimator, and a near-far problem mitigation technique.

I. INTRODUCTION

Indoor and dense urban positioning have received much attention recently, since they constitute one of the bottlenecks in the massive deployment of location services in mobile networks [1] boosted by the US FCC 911 mandate and the EU E112 recommendation. Global navigation satellite system (GNSS) positioning has turned out to be one of the most suited candidates to implement this kind of services [1], [2], [3]. However, as the other candidates, conventional GNSS-based techniques can experiment an important degradation in indoor and dense urban environments. This has motivated in recent years an increasing research activity on signal processing techniques for indoor GNSS receivers (see for example [1], [2], [4].)

The main limitations facing indoor GNSS-based positioning are due to the complex propagation of the GNSS signals indoors. This propagation is characterized by high signal attenuation, near-far problem appearance due to the different attenuation profiles followed by the incoming signals, severe multipath, and even non-line-of-sight conditions. Those are the cause of the poor performance shown by conventional GNSS receivers inside indoor locations.

To overcome the above-referred limitations, a number of signal processing techniques have been proposed in the last years. The signal high attenuation can be overcome by the joint use of coherent correlation and non-coherent integration. This technique has given rise to the so-called High Sensitivity GNSS (or GPS) Receiver [2], [4], [5]. These kind of receivers process long periods of signal. By the use of long non-coherent integration, they can achieve a very low sensitivity, and avoid the effect of bit transitions and clock drifts [5]. These receivers usually make use of Assisted-GNSS (or Assisted-GPS) [2] in order to determine the position, due to 1) the low time to fix required and 2) the impossibility to demodulate the navigation message in high-attenuation conditions. To overcome the near-

far problem, a number of well-known multiuser detection techniques for CDMA communications [6], [7], such as the decorrelation receiver, could be used, although they have a high computational burden. Thus, other more efficient methods have been proposed, e.g. the use of the time-varying behaviour of near-far interference to detect it [5], or the use of a near-far detector followed by interference cancellation suggested by the authors [8], [9]. Finally, the multipath can be mitigated by the use of multipath-resistant discriminators/interpolators or the estimation of the direct and reflected rays in a ray model [10].

This paper deals with the experimental test of the performance of some of the above-listed techniques and the study of some of the characteristics of the indoor propagation, such as the attenuation and the near-far problem. We use a one-shot receiver whose architecture was already described in previous authors' papers [8], [9]: This receiver consists of a high-sensitivity GNSS receiver using both coherent correlation and non-coherent integration, followed by near-far mitigation, a proper CN_0 estimation, and a location algorithm based on Assisted-GNSS [11]. Since it is a one-shot receiver, it works on a single block of GPS digitalised samples to reduce computational load, i.e. it only incorporates the acquisition stage of a standard receiver. Therefore, it seems to be very suitable to be integrated in a wireless device. Multipath mitigation is not treated in the paper. The rest of the paper is organised as follows, the high-sensitivity GNSS receiver is briefly reviewed in Section II. Section III describes the CN_0 estimation algorithm and the near-far mitigation technique, and Section IV shows the results coming from the measurements. The conclusions are drawn in Section V.

II. HIGH-SENSITIVITY GNSS RECEIVER STRUCTURE

High-sensitivity GNSS receivers [2], [4] combine coherent correlation and non-coherent integration during long periods of time of even seconds. Given a navigation signal $x(t)$ IQ demodulated in baseband, the high-sensitivity GNSS receiver computes the square cross-correlation between $x(t)$ and a delayed and modulated replica of the signal transmitted by the i th satellite:

$$X_i(\tau, f) = \frac{1}{N_I} \sum_{r=0}^{N_i-1} \left| \int_{rL_cT_cN_c}^{(r+1)L_cT_cN_c} x(t) c_i^*(t - \tau) e^{-j2\pi ft} dt \right|^2, \quad (1)$$

where N_c and N_I are the number of code epochs coherently correlated and the number of blocks incoherently integrated, respectively; T_c and L_c are the chip period and the code length. The coherent correlation time is then $L_c T_c N_c$, and the dwell time becomes $L_c T_c N_c N_I$. Signal $c_i(t)$ is the code replica corresponding to the signal of the i th satellite and accounts for the Doppler in the code, i.e.: $c_i(t) = \sum_r a_i(r) p_{T_c'}(t - r T_c')$, and $T_c' = T_c(1 + f/f_0)$; $a_i(r)$ is the code sequence corresponding to the i th satellite, f is the Doppler cell under test and f_0 the nominal GPS carrier frequency ($f_0 = 1575.42$ MHz).

The acquisition is then a parallel ($X_i(\tau, f)$ is computed on the same signal shot), two-dimensional, single-dwell procedure. The square cross-correlation is evaluated for a discrete grid of code delay and Doppler frequency values. The delay and Doppler estimates of the signal coming from the i th satellite are those values maximizing the square cross-correlation $X_i(\tau, f)$,

$$\left(\hat{\tau}_i, \hat{f}_i\right) = \arg \max\{X_i(\tau, f)\}. \quad (2)$$

The i th satellite is acquired when the maximum of the corresponding square cross-correlation, $X_i(\hat{\tau}_i, \hat{f}_i)$, surpasses a certain threshold defined for a given probability of false alarm P_{FA} .

In the one-shot receiver used, $X_i(\tau, f)$ is computed column-wise, i.e. for every Doppler cell, the incoming signal is demodulated and the value of the correlation for each correlation lag is obtained with the FFT. The resolution in time of the delay-Doppler grid will be thus the sampling period used by the receiver. The resolution in Doppler frequency will be inversely proportional to the coherent correlation time. The resolution in the code delay estimation can be nevertheless insufficient since the one-shot receiver will only include the acquisition stage. To further improve the code delay estimation without increasing much the sampling rate, interpolation can be used by considering the cross-correlation values around the code delay estimate $\hat{\tau}_i$ (at the same Doppler cell \hat{f}_i). Piecewise linear interpolation has been used. Further information about this method and other issues regarding high-sensitivity receivers can be found in [8]. Simulations have shown a good performance of this simple interpolation technique for both limited and non-limited bandwidth signals [8].

The effect of the bit transitions deserves special attention, since the use of long coherent correlation in the high sensitivity receiver can result in bit transitions mainly causing sensitivity losses. These losses are given, in mean and in the worst case, by

$$\bar{L} = -10 \log_{10} \left(1 - \frac{L_c T_c N_c}{3 T_b}\right), \quad (3)$$

$$L_{wc} = -10 \log_{10} \left(1 - \frac{L_c T_c N_c}{T_b}\right), \quad (4)$$

T_b being the bit period. Neither the mean nor the worst-case expressions depend on the number of blocks non-coherently integrated but on the coherent correlation time.

Further, L_{wc} becomes infinity when the coherent correlation time approaches T_b . Both expressions are valid for coherent correlation time below T_b and dwell times greater than T_b .

As pointed out in the Introduction, High sensitivity receivers and Assisted-GNSS are intimately related. The aim of Assisted-GNSS is to provide the information contained in the navigation message necessary to compute the position (satellite ephemeris, satellite clock corrections, approximate GPS time), "differential corrections" (mainly tropospheric and ionospheric corrections), and information to facilitate the indoor acquisition (list of visible satellites, Doppler range, even parts of the navigation message). All the information about the GPS system is collected by a GPS receiver on a reference station in the vicinity of the indoor receiver and transmitted to it via a mobile communication system. In the results presented in this paper, either a GPS receiver working outdoors or just the information contained in a rinex file have been played the role of the reference station.

III. CN_0 ESTIMATION AND NEAR-FAR PROBLEM

Let $\hat{\tau}_i$ and \hat{f}_i be the code delay (previous to interpolation) and Doppler frequency at which the i th satellite signal is acquired, and P the mean power of the received signal $x(t)$ within the dwell time, i.e. $P = \frac{1}{L_c T_c N_c N_I} \int_0^{L_c T_c N_c N_I} |x(t)|^2 dt$. The i th satellite CN_{0i} estimate is computed as

$$\widehat{CN}_{0i}(dBHz) = 10 \log_{10} \left(\frac{B_n X_i(\hat{\tau}_i, \hat{f}_i) - L_c T_c N_c P}{(L_c T_c N_c)^2 P - X_i(\hat{\tau}_i, \hat{f}_i)} \right). \quad (5)$$

This estimator is obtained by assuming only one satellite signal in noise of equivalent bandwidth B_n , and substituting P and $X_i(\hat{\tau}_i, \hat{f}_i)$ by their corresponding statistical mean values. That approximation is valid for large non-coherent integration. The bandwidth B_n accounts for every filtering that could have been done before acquisition. This estimator assumes zero multiaccess interference and should be conveniently modified under near-far problem conditions, i.e. P would then be the power of the incoming signal after the cancellation of the interference. Further information and its derivation can be found in [9] where it is shown how the estimator tends to the Cramer-Rao bound as the true CN_0 increases.¹

Regarding the near-far problem mitigation, we implement the algorithm proposed in [9] that is briefly described in the following. The algorithm comprises two steps: First, near-far problem detection; and second, near-far interference cancellation.

The near-far problem detector is based on the different statistical model of the square cross-correlation of (2) for zero and nonzero multiaccess interference (MAI). For zero MAI, the maximum of the square cross-correlation $X_i(\hat{\tau}_i, \hat{f}_i)$ will be dominated by noise for any code delay more than one chip away from the optimum one ($\hat{\tau}_i$) and the probability that

¹Note that Eqn. (8) in [9] and Eqn. (7) in [8] have a typing error in the definition of the CN_0 estimator.

$X_i(\tau, \hat{f}_i)$ surpasses a given threshold for any of those code delays can be theoretically computed. For nonzero MAI, the square cross-correlation $X_i(\tau, \hat{f}_i)$ will be dominated by the cross-correlation between the interfering signal and the code replica of the i th satellite signal, so that this probability P_E will be much higher than for zero MAI.

After detecting a satellite affected by nonzero MAI, the receiver skips the acquisition of that satellite and continues acquiring other visible ones. When the acquisition has finished, the multiuser technique is applied to each of the skipped satellite signals. The multiuser technique (interference cancellation) consists of computing an approximate orthogonal complement of the received signal to the subspace spanned by the satellite signals previously acquired [6], [12]. Only those holding a high CN_0 estimated value are used. Finally, the acquisition of the weak satellites is tried again by using the resultant orthogonal complement. This approach only requires one-shot of the signal and mitigates both on-frequency and off-frequency cross-correlation. Other approaches, such as [5], require two nonconsecutive signal shots and only deal with off-frequency cross-correlation; and those purely based on multiuser estimation algorithms have a greater computational burden.

IV. RESULTS

Live raw GPS samples have been collected by the NordNav R30 software receiver. Samples are recorded at 16.3676 MHz sampling rate, 4.1394 MHz intermediate frequency, 3 MHz bandwidth and 4 bits quantisation. The NordNav R30 clock is a conventional TCXO with a 0.5ppm stability. Off-line pre-processing demodulates, filters, and decimates (by 3: sampling frequency 5.4558 MHz) the sampled signal. Preprocessed recordings have been analysed by one-shot receivers with different configurations varying the coherent correlation time and number of blocks non-coherently integrated. Table I shows all the tested configurations along with their corresponding sensitivity defined as the minimum CN_0 for a satellite signal to be acquired for the receiver assuming 10^{-8} false alarm probability and 90% detection probability (per decision). This value of false alarm probability leads to a false alarm probability per searched satellite around 10^{-5} . Sensitivity in Table I does not take into account the losses due to transitions of the navigation message bits [8]. Mean losses would be 1.5 dB for the 15 ms coherent interval and less for the rest.

A. Dataset Inlab2

Dataset **Inlab2** was collected in the European Navigation Laboratory, at ESTEC, Noordwijk, The Netherlands, on June, the 6th 2004, at 9:06 am. One minute of GPS L1 C/A signal was recorded. For the sake of processing, the record was split into independent shots of duration equal to the dwell time required for the receiver configuration tested. The corresponding arrangement of the visible GPS satellites in azimuth and elevation is plotted in Fig. 1 along with the layout of the room within which the measurement was carried out. The room is on the first floor of a 1-storey building and its

window is oriented towards 230° . Figure 2 shows the CN_0 estimate of the satellites acquired along the different shots comprising the one-minute long recording for 10ms coherent correlation and 500-block non-coherent integration. As can be noticed, satellites SV22, SV14, SV3, SV15 and SV11 are the most powerful received ones, and according to Fig. 1 the first four come through the external wall and SV11 does through the window. They suffer from between 20 and 30 dB losses if compared with the CN_0 estimated for dataset **Outlab2** taken outdoors on the laboratory roof right after dataset **Inlab2** was recorded (see Fig. 2). Note that the receiver configuration for the dataset **Outlab2** is merely a 1ms coherent correlation.

The above-referred losses are also contributed by the antenna used, a Mighty Mouse II fed at 3.3 V. The higher losses of SV11 may well be due to diffraction and partial blocking since there are other buildings on its way. The composition of the roof is really lossy given that SV19, the satellite with highest elevation, is acquired only in 4 out of 11 shots, and at a quite low CN_0 (19 dBHz).

Figure 4 represents the absolute error of the position fix computed by Assisted-GNSS with respect to the true position of the receiver (given by the NordNav R30 receiver working outdoors). Values below 150 m are easily obtained. Interestingly, it seems that better fixes are obtained with lower dwell times. However, configurations with low dwell time are able to acquire less likely the at-least 5 satellites required for the Assisted-GNSS to compute the fix. The availability of fix for dataset **Inlab2** and the configuration tests is shown in Table II. For instance, with 10ms coherent correlation and 500-blocks non-coherent integration there is a fix for all the shots; however, with 5ms coherent correlation and 200-blocks non-coherent integration a fix can be computed only in 50% of the shots. On the contrary, this does not occur for the outdoors counterpart: As can be noted in Fig. 5, higher dwell time configurations give rise to lower positioning errors. (The position fix for dataset **Outlab2** is also computed by means of Assisted-GNSS.) This may well be due to the fact that long dwell times indoors make it possible to acquire very weak satellites that 1) hold a higher error in the code delay estimation, 2) have likely suffered more than the stronger satellites from typical indoor propagation mechanism, such as multipath. (Note that multipath mitigation is beyond the scope of this paper.) Connected to this issue, Figs. 6 and 7 plot the error of the fixes represented in a local coordinate system centred at the true position. Only coordinates X (East-West) and Y (North-South) are depicted; coordinate Z would correspond to the height. As can be noticed, the indoor fixes have a bias which is not observed in the outdoor ones.

For the configuration of 10ms coherent correlation and 500-block non-coherent integration, Fig. 4 shows two error curves: one including SV28 when it is acquired and the other one without SV28. In general, the exclusion of SV28 improves the position fix. Figure 8 depicts the normalised cross-correlation between the incoming indoor signal and the receiver code replica of the acquired satellites along the correlation lags for two shots with 10ms coherent correlation and 500-blocks

TABLE I

TESTED ONE-SHOT RECEIVER CONFIGURATION AND CORRESPONDING SENSITIVITY, I.E. MINIMUM CN_0 (DBHZ) FOR 10^{-8} FALSE ALARM PROBABILITY AND 90% DETECTION PROBABILITY (PER DECISION).

Configuration	Sensitivity (dBHz)
Coherent correlation: 5 ms, Non-coherent Int.: 200 blocks. Dwell time: 1 sec	20.4
Coherent correlation: 10 ms, Non-coherent Int.: 200 blocks. Dwell time: 2 sec	17.4
Coherent correlation: 10 ms, Non-coherent Int.: 500 blocks. Dwell time: 5 sec	15.2
Coherent correlation: 15 ms, Non-coherent Int.: 2000 blocks. Dwell time: 30 sec	10.3

TABLE II

AVAILABILITY OF 5 OR MORE ACQUIRED SATELLITES TO COMPUTE THE POSITION FIX VIA ASSISTED-GNSS FOR THE DATASET **Inlab2**.

Configuration	Availability (%)
Coherent correlation: 5 ms, Non-coherent Int.: 200 blocks. Dwell time: 1 sec	50
Coherent correlation: 10 ms, Non-coherent Int.: 200 blocks. Dwell time: 2 sec	80
Coherent correlation: 10 ms, Non-coherent Int.: 500 blocks. Dwell time: 5 sec	100

non-coherent integration: Shot 1 goes from 0 to 5 sec of the recording and Shot 3 from 10 to 15 sec. In the correlation for Shot 3, SV28 appears and its main lobe tends to widen in the left-hand side. This may suggest some sort of multipath mechanism that can cause an error in its code delay estimation. In connection to this, the fix absolute error for Shot 3 is 400 m if SV28 is used, and becomes around 50 m if excluded. For the sake of completeness, Fig. 9 shows the error in the pseudoranges estimated by Assisted-GNSS with 10ms coherent correlation and 500-blocks non-coherent integration and dataset **Inlab2**. It has been computed by assuming a linear model for the pseudoranges, which makes sense given the short duration of the dataset. It can be noticed that the times with high pseudorange errors coincide with the one of high absolute positioning errors (see Fig. 4, curve for 10ms coherent correlation and 500-block non-coherent integration including SV28).

The errors obtained are also due to the need to estimate the GPS receiver time when the Assisted-GNSS is used. In order to solve the 1ms ambiguity that the Assisted-GNSS has, the positioning equation is solved for time instants separated multiples of 1 ms from the initial GPS time estimate of the receiver [11]. Then the residual of the positioning equation is computed and the final GPS time estimate is the one corresponding to the minimum residual value. Figure 10 shows the residual for each 1ms ambiguity interval around the initial GPS time estimate. The minimum of the residual would correspond to the selected receiver GPS time. Nevertheless, it can be noticed that this minimum does not coincide with the minimum of the positioning error with regard to the true position; thus the selected GPS time does not lead to the minimum positioning errors. Also note that the minimum of the positioning error is narrow (y axis expressed in logarithmic units), so that deviations of several milliseconds between both minima would give rise to high positioning errors. Figure 11 illustrates the magnitude of the error in the receiver time estimation: It shows the difference in receiver time estimate between consecutive shots. Given the receiver configuration (10ms coherent correlation and 500-block non-coherent inte-

gration), this difference should be 5 sec. However, it oscillates around that value and can even deviate in tens of milliseconds.

TABLE III

ABSOLUTE POSITIONING ERROR (IN METRES) FOR 15MS COHERENT CORRELATION AND 2000-BLOCK NON-COHERENT INTEGRATION.

DATASET **Inlab7**.

Shot 1	Shot 2
18.71	63.49

B. Dataset Inlab7

Dataset **Inlab7** was collected in the room Ca227 at ESTEC, Noordwijk, The Netherlands, on February, the 2nd 2005, at 4:33 pm. One minute of GPS L1 C/A signal was recorded. The room is on the second floor of a 4-storey building and its window is oriented towards 280° and is 3.5m wide; the receiver was placed 5 m away from the window. On the window direction, there are some hills blocking the reception of satellites below 15° elevation. This environment is deeper indoor than the one considered in the previous section. Therefore, a long dwell time configuration has been used: a 15ms coherent correlation followed by the non-coherent integration of 2000 blocks. That is, the dwell time is 30 sec, so that only 2 shots can be taken from the recording. The sensitivity of this receiver configuration is 10.3 dBHz (Table I). The position of the visible GPS satellites in the sky is shown in Fig. 12 along with the approximate arrangement of the room (room layout not in scale). Figure 13 shows the normalised cross-correlation for the satellites acquired in the 1st shot. It is also shown the corresponding CN_0 estimate, which ranges from 32.8 (SV8) to 11.5 dBHz (SV11). For Shot 2, the results obtained are similar. It seems that the most powerful received satellites, SV8 and SV19 comes through the window. The rest of them, but SV11, come through windows in the eastern side of the building on the same floor. Satellite SV11 is also believed to arrive through the window although it may experience partial blocking due to the existence of other buildings. The absolute error of the fixes are very low for both shots, as can be seen in Table III.

Dataset **Inlab8** was collected in the meeting room Df304 at ESTEC, Noordwijk, The Netherlands, on June, the 1st 2005, at 7:00 pm. One minute of GPS L1 C/A signal was recorded. For the sake of processing, the record was split in independent shots of duration equal to the dwell time required for the receiver configuration tested. The corresponding arrangement of the visible GPS satellites in azimuth and elevation is plotted in Fig. 14 along with the layout of the room within which the measurement was carried out (not in scale). The room is on the 3rd floor of a 3-storey building and its large window is oriented toward 230°. Figure 15 shows the normalised correlation of the acquired satellites for Shot 1 (configuration: 10ms coherent correlation and 500-block non-coherent integration). Clearly, there is a dominant satellite (SV10) coming through the window. There are also two satellites, SV28 and SV19, with remarkable CN_0 arriving also through the window (SV28) or through the window on the other side of the building (SV19). Satellites SV8, SV26, SV27 and SV29 are likely received through the roof and walls. Note that the correlation of SV3 has many important secondary lobes. Actually this satellite would correspond to a false acquisition appearing due to the multiaccess interference coming from the dominant satellite. This situation is detected by the near-far detector, then the dominant satellite is cancelled from the signal samples, and the SV3 is no longer acquired afterwards, i.e. it appeared as a false acquisition before applying the near-far mitigation algorithm. This happens to SV3 in all the shots, and also to SV8 in some shots. To illustrate the near-far interference from the dominant satellite also on SV8, Fig. 16 shows the cross-correlation for Shot 7. Both SV3 and SV8 are no longer detected after the dominant satellite cancellation, since they do not arrive with enough power, i.e. they were falsely acquired before near-far mitigation due to the cross-correlation from the dominant satellite code. If the position had been computed before near-far mitigation, the positioning error could have reached thousands of kilometres. However, after the Near-Far mitigation algorithm this error is below 150 m for all shots (10ms coherent correlation and 500-blocks non-coherent integration), as depicted in Fig. 17.

V. CONCLUSIONS

The performance of a one-shot high-sensitivity GNSS receiver has been evaluated by measurements. The receiver is a software one, it works off-line, processes the GPS L1 C/A signal, and uses Assisted-GNSS to solve the positioning equation. The analysis has been carried out both from the signal processing (correlation and CN_0) and from the positioning accuracy perspectives. The receiver also includes a CN_0 estimator and a near-far mitigation algorithm.

Most of the measurements have been carried out in medium indoor environments, where some satellites reach the receiver through windows or just one external wall, and there is likely to find 5 or more satellites above 20 dBHz. For this type of environments, a 5-sec dwell time (10ms coherent correlation and 500-block non-coherent integration) seems to be sufficient

to guarantee an 100% availability of position fix for any signal shot. The positioning error have been lower than 150 m in most of the fixes.

A deeper indoor environment has been also tested in which it was necessary to acquire satellites with a CN_0 down to 11 dBHz. That required a 30-sec dwell time configuration (15ms coherent correlation and 2000-block non-coherent integration). That configuration could be not very practical, so that new assisted techniques may come into play: For instance, the extension of the coherent correlation time beyond the bit period by providing the navigation bits. This could be possible at the expense of a higher computational burden and higher quality clock in the receiver and would required more accurate Assisted-GNSS data (Doppler information) and an more precise synchronisation of the receiver (better estimate of the receiver GPS time before running Assisted-GNSS). Another element degrading the incoming CN_0 may be the antenna: The use of a better one is currently under test, although it may not faithfully reproduce the conditions of real indoor users.

An example of near-far problem has been shown and the consequences of not handling it pointed out. This problem will appear often in medium indoor conditions, since some of the satellites can suffer from much less losses due to propagation through windows. The proposed technique has shown to behave appropriately detecting those satellites suffering from high interference levels.

Another important issue treated has been the synchronisation of the receiver. The limitations of the Assisted-GNSS technique to estimate jointly the position and receiver time has been pointed out. A better synchronisation of the receiver could help to reduce the positioning error as well as to alleviate the computational burden of the Assisted-GNSS algorithm.

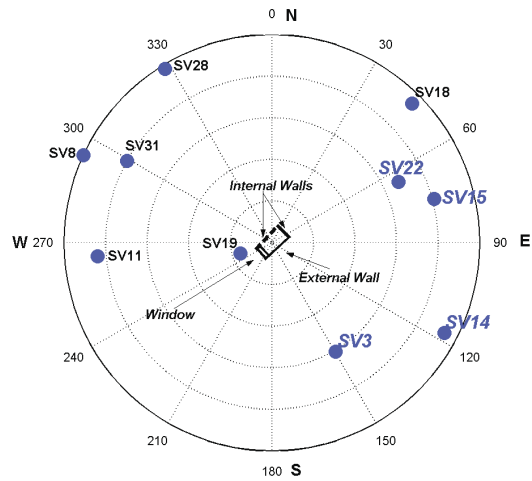
ACKNOWLEDGMENTS

The work of G. López-Risueño has been supported by the ESA Spanish Trainee Programme funded by the Spanish Ministry of Science and Education.

REFERENCES

- [1] K. Pahlavan, X. Li, and J.-P. Mäkelä. Indoor Geolocation Science and Technology. *IEEE Communications Magazine*, pages 112–118, Feb 2002.
- [2] F. van Diggelen. Indoor GPS Theory & Implementation. In *IEEE Position, Location & Navigation Symposium 2002*, pages 240–247, 2002.
- [3] Coordination Group on Access to Location Information for Emergency Services (CGALIES). Implementation Issues related to Access to Location Information by Emergency Services (e112) in the European Union. Technical report, CGALIES, 2002. <http://www.telematica.de/cgalies/main.html>.
- [4] G. Lachapelle, H. Kuusniemi, D. T. H. Dao, G. MacGougam, and M. E. Cannon. HSGPS Signal Analysis and Performance under Various Indoor Conditions. In *ION GPS/GNSS 2003*, pages 1171–1184, Sept 2003.
- [5] G. P. Mattos. Solutions to the Cross-Correlation and Oscillator Stability Problems for Indoor C/A Code GPS. In *ION GPS/GNSS 2003*, pages 654–659, 2003.
- [6] S. Verdu. *Multiuser Detection*. Cambridge University Press, 1998.
- [7] S. Parkvall, E. Ström, and B. Ottersten. The Impact of Timing Errors on the Performance of Linear DS-CDMA Receivers. *IEEE Journal on Selected Areas in Communications*, 14(8):1660–1668, October 1996.

- [8] G. López-Risueno and G. Seco-Granados. Measurement and Processing of Indoor GPS Signals Using a One-Shot Software Receiver. In *2nd ESA Workshop on Satellite Navigation User Equipment Technologies (NAVITEC'2004)*, 2004.
- [9] G. López-Risueno and G. Seco-Granados. CNo Estimation and Near-Far Mitigation for GNSS Indoor Receivers. In *IEEE Vehicular Technology Spring Conference (VTC Spring 2005)*, 2005.
- [10] J. Soubielle, I. Frijalkow, P. Duvaut, and A. Bibaut. GPS Positioning in a Multipath Environment. *IEEE Trans. on Signal Processing*, 50(1):141–150, Jan. 2002.
- [11] J. Syrjärinne. Possibilities for GPS Time Recovery with GSM Network Assistance. In *Proc. ION GPS*, pages 955–966, Sept 2000.
- [12] P. H. Madhani, P. Axelrad, K. Krumvieda, and J. Thomas. Application of Successive Interference Cancellation to GPS Pseudolite Near-Far Problem. *IEEE Trans. on Aerospace and Electronic Systems*, 39(2):481–488, April 2003.



Dataset Inlab2 @ European Navigation Lab, 6 June 2004, 9:06am. 1st floor out of a 1-storey building

Fig. 1. Satellite Polar Plot and room arrangement (not in scale). Dataset **Inlab2**.

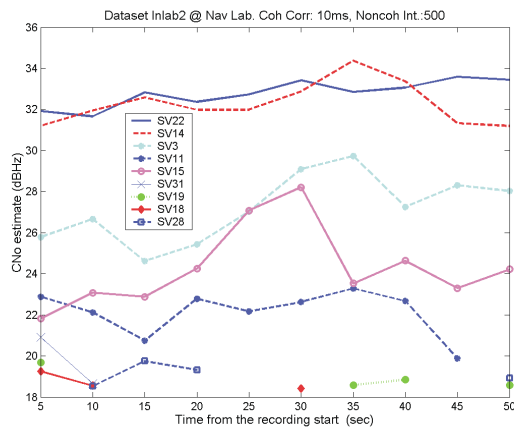


Fig. 2. CN_0 estimate for a 10ms coherent correlation and a 500-block non-coherent integration. Dataset **Inlab2**.

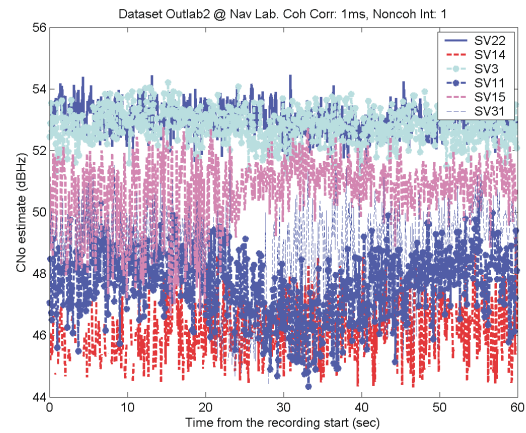


Fig. 3. CN_0 estimate for a 1ms coherent correlation. Dataset **Outlab2**.

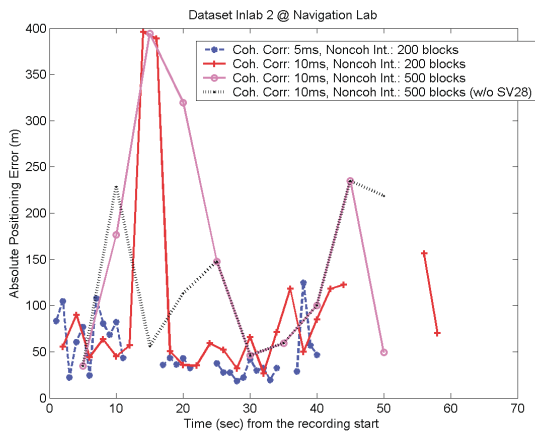


Fig. 4. Absolute Positioning Error. Dataset **Inlab2**.

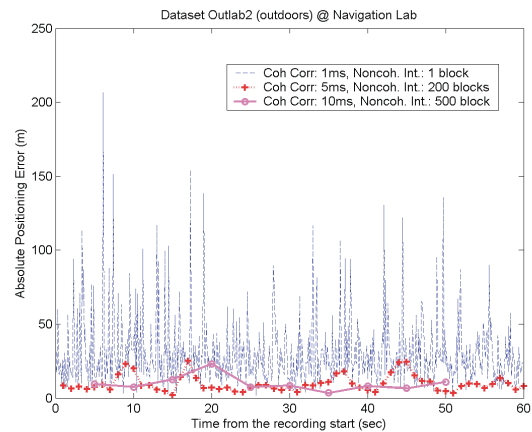


Fig. 5. Absolute Positioning Error. Dataset **Outlab2**.

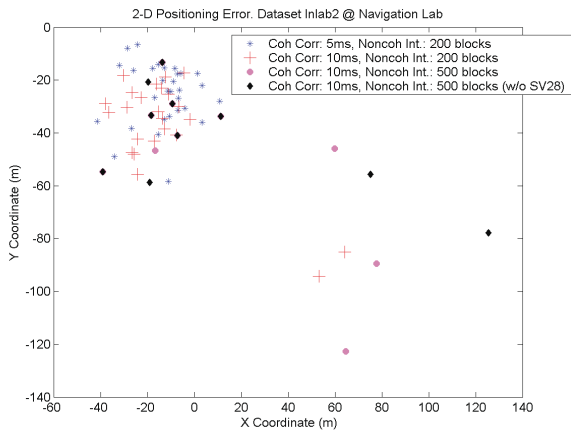


Fig. 6. Projection of the positioning error in the coordinates X (East-West) and Y (North-South) relative to the true position. Dataset **Inlab2**.

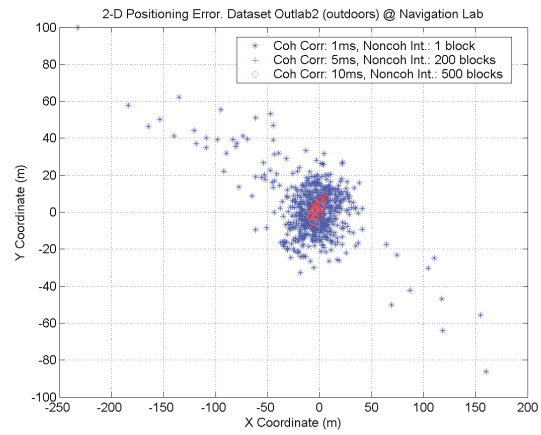


Fig. 7. Projection of the positioning error in the coordinates X (East-West) and Y (North-South) relative to the true position. Dataset **Outlab2**.

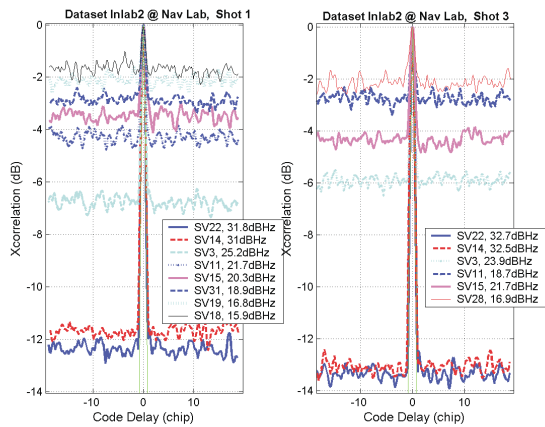


Fig. 8. Normalised cross-correlation for Shots 1 and 3 for the receiver configuration: 10ms coherent correlation and 500-block non-coherent integration. Dataset **Inlab2**.

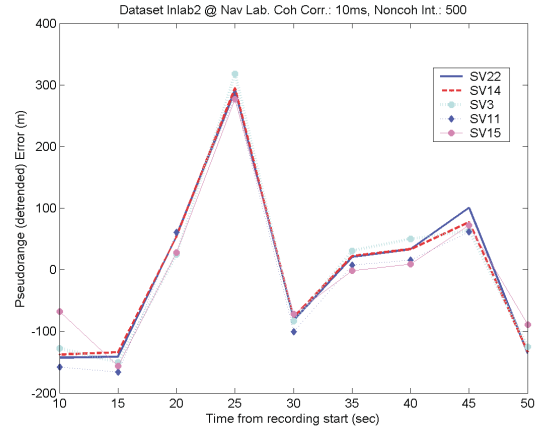


Fig. 9. Error in the Pseudoranges for a 10ms coherent correlation and a 500-block non-coherent integration. Dataset **Inlab2**.

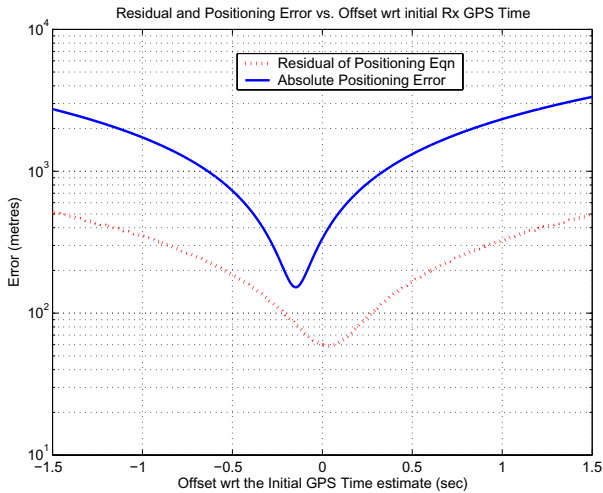


Fig. 10. Assisted-GNSS residual versus time ambiguity for a 10ms coherent correlation and a 500-block non-coherent integration. Dataset **Inlab2**, Shot 3 (with SV28).

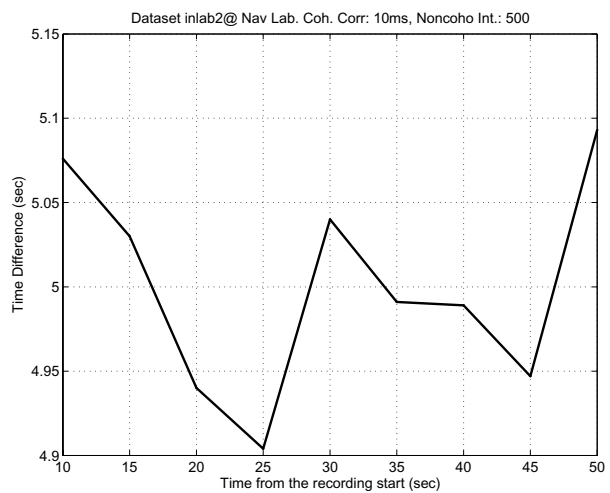
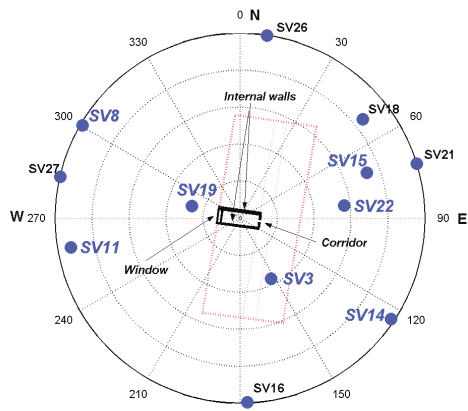
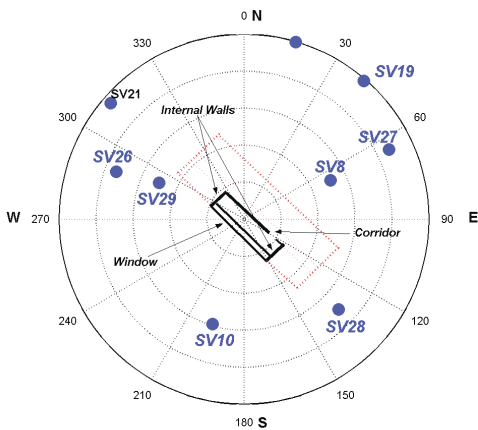


Fig. 11. Time difference between consecutive shots for a 10ms coherent correlation and a 500-block non-coherent integration (with SV28). Dataset **Inlab2**.



Dataset Inlab7 @ Room Ca227, 2 February 2005, 4:33am. 2nd floor out of a 4-storey building

Fig. 12. Satellite Polar Plot and room arrangement (not in scale). Dataset **Inlab7**.



Dataset Inlab8 @ Meeting room Df304, 1 June 2005, 7:00pm. 3rd floor out of a 3-storey building.

Fig. 14. Satellite Polar Plot and room arrangement (not in scale). Dataset **Inlab8**.

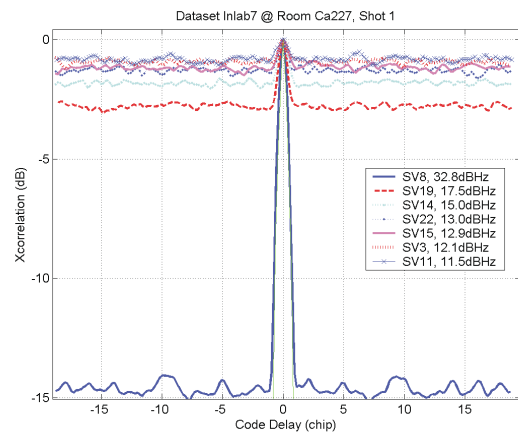


Fig. 13. Normalised cross-correlation for the 1st shot for the receiver configuration: 10ms coherent correlation and 500-block non-coherent integration. Dataset **Inlab7**.

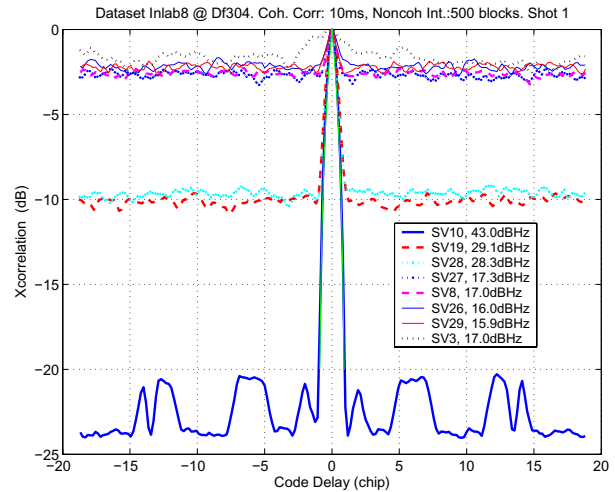


Fig. 15. Normalised cross-correlation for the 1st shot for the receiver configuration: 10ms coherent correlation and 500-block non-coherent integration. Dataset **Inlab8**. SV3 is not a true acquisition but the effect of the SV10 interference. (This is correctly handled by the near-far mitigation algorithm).

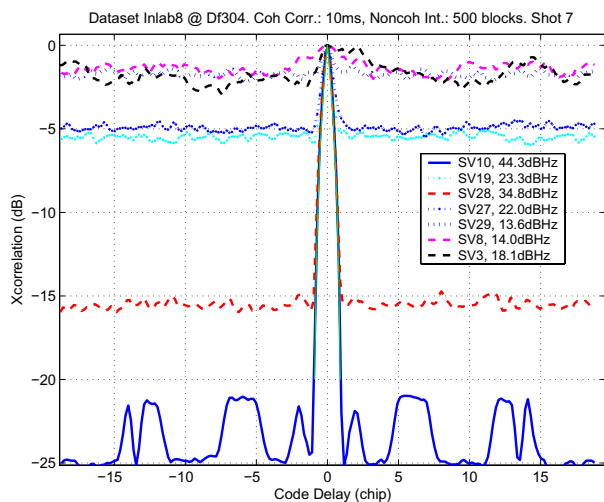


Fig. 16. Normalised cross-correlation for the 7th shot for the receiver configuration: 10ms coherent correlation and 500-block non-coherent integration. Dataset **Inlab8**. SV3 and SV8 do not correspond to true acquisition, but they are the effect of the SV10 interference. (This is correctly handled by the near-far mitigation algorithm).

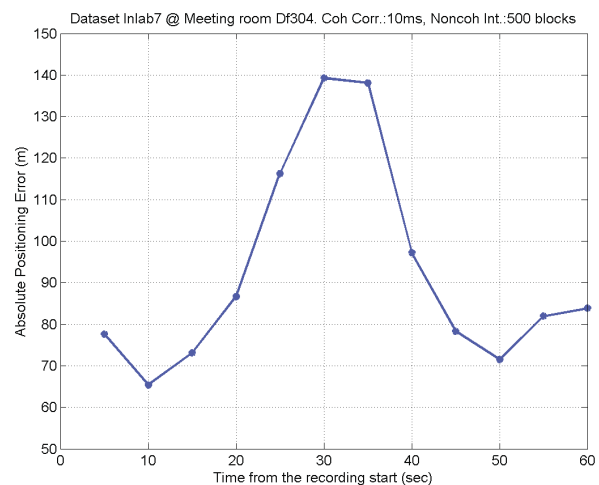


Fig. 17. Absolute Positioning Error. Dataset **Inlab8**.